Bull. Mater. Sci., Vol. 33, No. 4, August 2010, pp. 357–364. © Indian Academy of Sciences.

Temperature dependent growth and optical properties of SnO_2 nanowires and nanobelts

S P MONDAL, S K RAY*, J RAVICHANDRAN† and I MANNA†

Department of Physics & Meteorology, Indian Institute of Technology, Kharagpur 721 302, India
†Department of Metallurgical & Materials Engineering, Indian Institute of Technology, Kharagpur 721 302, India

MS received 10 February 2009; revised 14 February 2010

Abstract. **SnO_2 nanowires and nanobelts have been grown by the thermal evaporation of Sn powders. The growth of nanowires and nanobelts has been investigated at different temperatures (750–1000°C). The field emission scanning electron microscopic and transmission electron microscopic studies revealed the growth of nanowires and nano-belts at different growth temperatures. The growth mechanisms of the formation of the nanostructures have also been discussed. X-ray diffraction patterns showed that the nanowires and nanobelts are highly crystalline with tetragonal rutile phase. UV-visible absorption spectrum showed the bulk bandgap value (~3·6 eV) of SnO_2. Photoluminescence spectra demonstrated a Stokes-shifted emission in the wavelength range 558–588 nm. The Raman and Fourier transform infrared spectra revealed the formation of stoichiometric SnO_2 at different growth temperatures.**

Keywords. **SnO_2; nanostructures; growth mechanism; optical properties.**

1. Introduction

One-dimensional (1D) oxide nanostructures such as wires, rods, belts, and tubes have become the focus of intensive research owing to their unique applications in mesoscopic physics and fabrication of nanoscaled devices. They not only provide a good system to study the electrical and thermal transport in one-dimensional confinement, but also are expected to play an important role in fabricating electronic, optoelectronic, and magnetic storage devices with nanoscale dimension (Xia *et al* 2003). Tin oxide is an important functional material, which has been widely applied in the field of opto- and microelectronics, such as solar cells (Ferrere *et al* 1997), transparent conducting electrodes (He *et al* 1993), gas sensors (Ansari *et al* 1997; Varghese and Malhotra 1998), and transistors (Duan *et al* 2001). The synthesis and assembly of 1D SnO_2 nanostructures such as wires and belts have attracted great interest due to their unique applications in gas sensors and field-effect transistors (Comini *et al* 2002; Kolmakov *et al* 2005; Dattoli *et al* 2007). There are several methods for the synthesis of SnO_2 nanowires and belts such as chemical vapour deposition (Ma *et al* 2004; Calestani *et al* 2005), thermal evaporation (Pan *et al* 2001; Wang *et al* 2004; Duan *et al* 2005; He *et al* 2006) and different chemical synthesis routes (Zheng *et al* 2001; Her *et al* 2006). In this paper, we report the growth of SnO_2 nanowires and nanobelts on silicon substrates through a vapour–liquid–solid (VLS) mechanism by the evaporation of Sn powders at different temperatures. It has been observed that the nanostructures undergo shape transformation from wire to belt with the increase of growth temperature. The possible growth mechanism of formation of nanowires and nanobelts has been discussed. Microstructural and optical behaviours of the grown nanostructures have been investigated in detail.

2. Experimental

The synthesis of SnO_2 nanowires was based on thermal evaporation of Sn powders, under controlled conditions with the assistance of a gold catalyst. A fixed amount of Sn powder (99·99%) taken on a quartz boat was placed at the centre of a horizontal quartz tube furnace. Several *p*-type (100) silicon substrates coated with 18 nm gold films were used as the substrates and placed on the top at the downstream end of the boat. The growth of nanowires was carried out at temperatures, varying from 750–1000°C for 30 min with a constant flow of nitrogen at the rate of 100 sccm.

The field-emission scanning electron micrographs (FESEM) of the grown samples were recorded using a ZEISS SUPRA 40 system. Transmission electron microscopy (TEM) study was performed using a JEOL JEM-2100F microscope with an accelerating voltage of 200 kV. For the TEM analysis, the nanowires were dispersed ultrasonically in acetone and a drop of the solution

*Author for correspondence (physkr@phy.iitkgp.ernet.in)

was taken on a carbon coated copper grid. X-ray diffraction spectra were recorded by a Philips X-Pert PRO-MRD diffractometer with CuKα ($\lambda = 0{\cdot}15418$ nm) radiation operated at 45 kV and 40 mA with a grazing incidence 2·0°. UV-visible absorption spectra of the samples were studied in the wavelength range 200–800 nm to determine the bandgap using a Perkin-Elmer Lambda 45 spectrophotometer. Room temperature photoluminescence measurements (PL) were carried out using a He–Cd laser of wavelength, 325 nm and a Triax 310 monochromator. The emission was detected by a multi-channel photomultiplier detector. Fourier transmission infrared absorption spectra (FTIR) were recorded using a Nicolet NEXUS–870 spectrometer in the wave number range 4000–400 cm^{-1}. Raman spectroscopy of the samples was studied using a Renishaw Raman imaging 2000 spectrometer with an Ar-ion laser of wavelength, 514 nm.

3. Results and discussion

3.1 *Microstructural studies*

The nanowires were grown at four different growth temperatures such as 750, 850, 950 and 1000°C. For the microstructural studies, the as-deposited films were directly transferred to the FESEM chamber without disturbing the original nature of the deposited white wool-like products on the Au coated surface. Figure 1 shows the FESEM micrograph of SnO_2 samples grown at 750°C. It is evident from the micrograph that at this temperature there is no perceptible growth of nanowires. However, a very few nanorods of diameter, 50–60 nm and length around 200 nm are observed (inset of figure 1). On increasing the growth temperature to 850°C, a large quantity of nanowires of diameter, 150–200 nm and length, 6–8 μm, are observed (figure 2). As shown in the inset of figure 2(a), a gold tip is clearly visible at the end of the nanowire, which indicates that VLS mechanism indeed governs the growth of these nanowires. Interestingly, at 850°C, secondary branches (shown by arrows in figure 2b) from some nanowires have been observed. More importantly, these secondary branches always ended in a gold tip indicating a growth mechanism which is invariant of VLS process. Figure 3 shows the formation of SnO_2 nanobelts (grown at 950°C) having length more than 16 μm and width, 100–110 nm. In this growth temperature several branched structures have also been observed which are clearly shown by the arrows in figure 3(b). Figure 4 shows the growth of SnO_2 nanobelts of length, 80 μm to few mm at 1000°C. Figure 5(a) shows bright field TEM image of the SnO_2 nanowire synthesized at 850°C temperature of diameter around 200 nm and a gold nanoparticle is clearly observed at the tip of the nanowire. However, figure 5(b) revealed the TEM micrographs of belts-like structures grown at 950°C. The widths of the nanobelts are estimated from the micrographs as 100–200 nm. Inset of figure 5(b) shows the TEM micrograph at a junction position of a

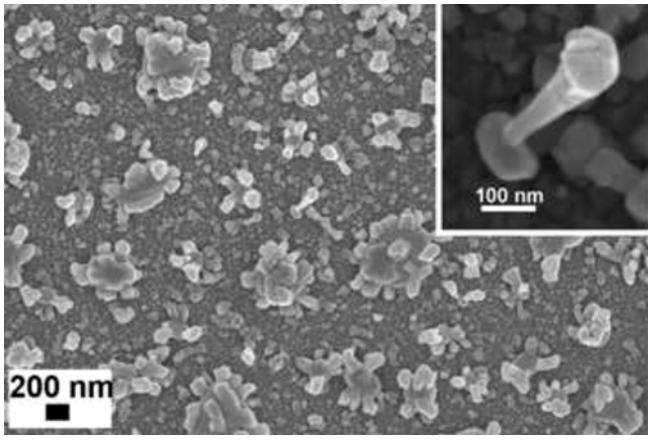

Figure 1. SEM micrographs of SnO_2 nanowires and a single nanowire of diameter 50–60 nm (inset) grown at 750°C temperature.

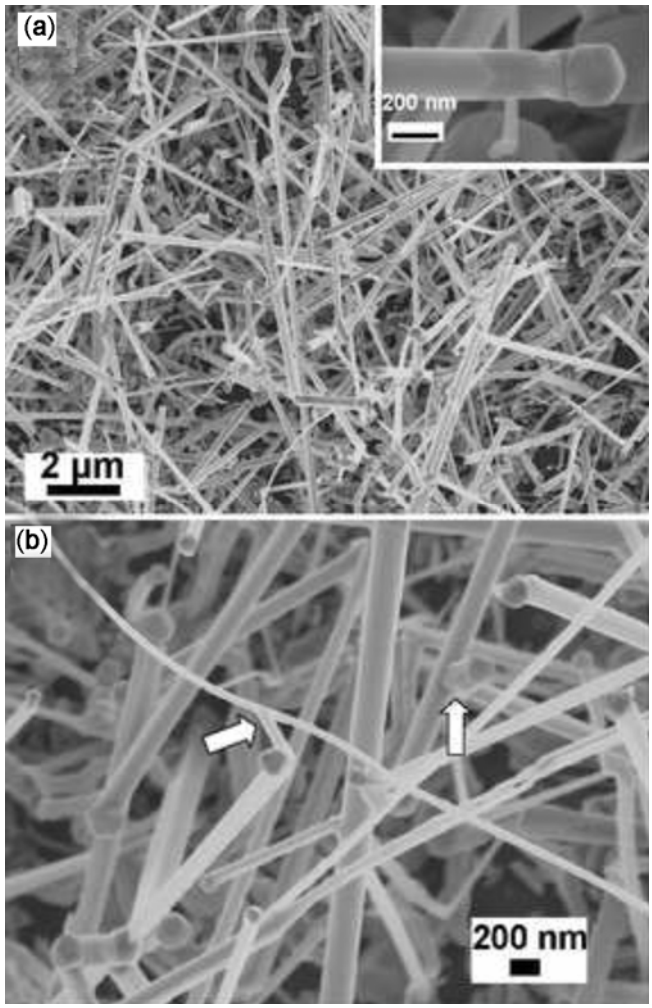

Figure 2. SEM micrographs of SnO_2 nanowires grown at 850°C temperature: (**a**) an assembly of nanowires, a single nanowire (inset) and (**b**) nanowires with several branches indicated by the arrows.

branched nanobelt. Figure 5(c) shows TEM micrograph of a nanobelt grown at 1000°C and the inset of this figure is the end portion of it. At 1000°C, the thickness, width and length of the nanobelts increases significantly, which is cleared from the FESEM as well as TEM micrographs. Interestingly, at this growth temperature the width to thickness ratio decreases and they show beam-like structure (figure 5(c)). It is more important that the width to thickness ratio of the nanobelts are not uniform along the length and it increases and finally ends at a gold tip. In this case the gold nanoparticle is clearly observed. Figure 5(d) shows the typical selected area electron diffraction (SAED) pattern of the nanobelts grown at 1000°C. The diffraction pattern indicates the nanobelts are single crystalline with (101) orientation, which is thermodynamically more favourable for SnO_2 nanostructures (Dai *et al* 2001; Beltran *et al* 2003).

3.2 *Growth mechanism*

There are two well established methods for the growth of nanowires, nanobelts and nanoribbons, the catalyst assisted vapour–liquid–solid (VLS) (Wagner and Ellis 1964; Wu and Yang 2001) and vapour–solid (VS) (Sears 1955; Yang and Lieber 1997; Pan *et al* 2001) methods. In the VLS process, the thin layer of deposited Au catalyst breaks up to form liquid nanodroplets at high temperature. These metal droplets form a liquid phase with the incoming molecular vapours above the eutectic temperature and finally, upon supersaturation of the solute species, nanowires start growing with the metal nanoparticles at their tips. Thus, a key signature of the VLS growth process is the presence of the metal nanoparticles at the tips of the nanostructures. On the other hand, in the VS method, the source materials vapourize to the molecular level with stoichiometric cation–anion molecules, which condense on the substrate and the molecules are arranged in such a way that the proper local charge balance and the structural symmetry are maintained, resulting in nucleation centres. With increasing molecular flux, the surfaces that have lower energy start to form and the low energy surfaces tend to be flat. Actually, in a VS growth process, the side surfaces of nanobelts or nanoribbons are essentially in thermodynamic (or atleast metastable) equilibrium with each other, therefore, this process is mainly

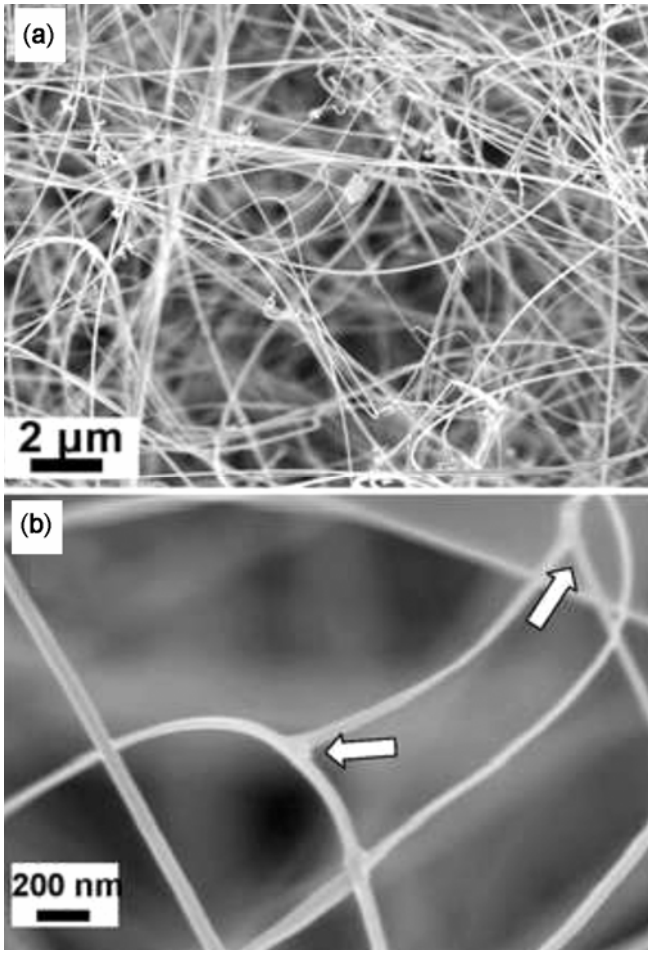

Figure 3. SEM images of SnO_2 nanobelts prepared at 950°C temperature: (**a**) a large view and (**b**) several branches of nanobelts indicated by the arrows.

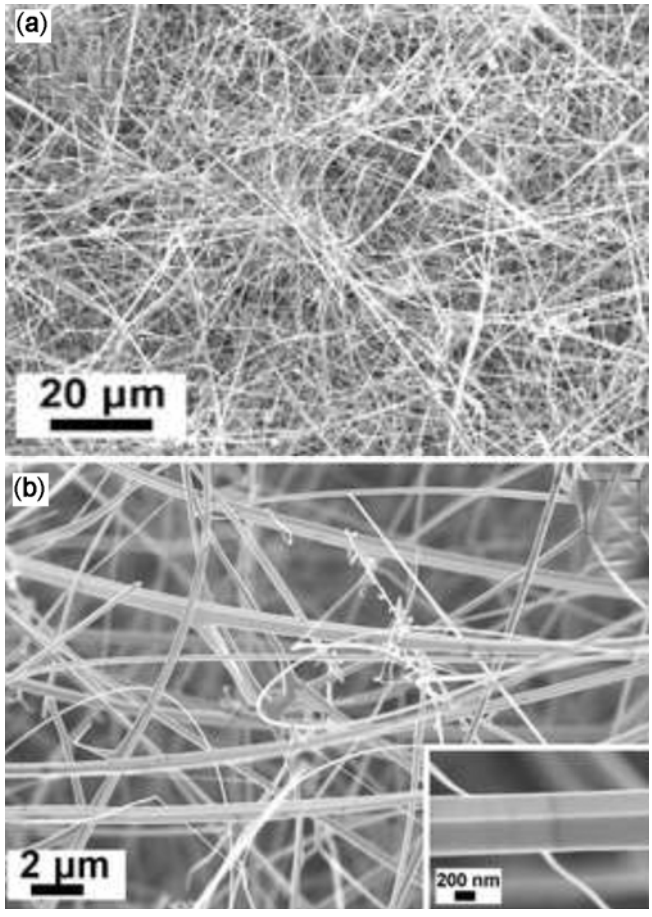

Figure 4. SEM micrographs of SnO_2 nanobelts at 1000°C growth temperature: (**a**) a large view and (**b**) magnified image and a rectangular shaped nanobelt (inset).

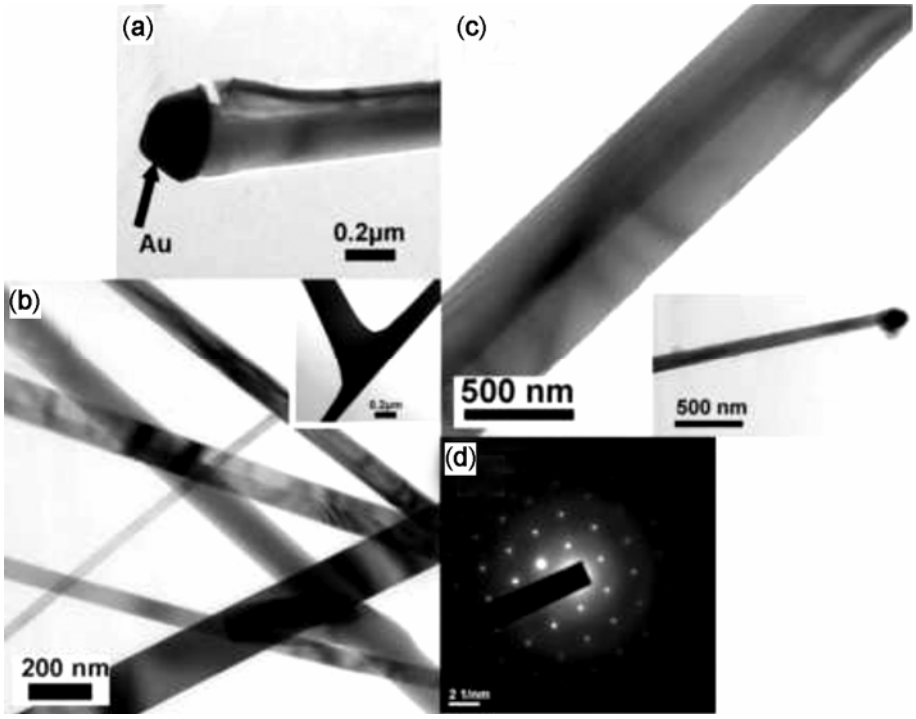

Figure 5. (**a**) Typical bright field TEM image of a single nanowire grown at 850°C, (**b**) TEM image of SnO_2 nanobelts grown at 950°C and inset of the figure represents a Y-junction nanobelt, (**c**) typical TEM micrograph of a SnO_2 nanobelt and its end portion (inset) synthesized at 1000°C and (**d**) selected area electron diffraction pattern of a nanobelt grown at 1000°C.

thermodynamically controlled (Beltran *et al* 2003). In this study, we believe that the nanowire arrays grow following the VLS mechanism, whereas for the SnO_2 nanobelts both the VLS and VS processes are equally dominant for the evolution of the typical morphology. As mentioned earlier, for growth temperatures between 750 and 850°C, the observed Au metal nanoparticles at the end of each nanowire, confirms the vapour–liquid–solid mechanism. Figure 6(a) shows the schematic diagram of the proposed growth mechanism of SnO_2 nanowires by VLS process. However, at 850°C, a number of nanowires with branched structure have been observed, which are indicated by the arrows in figure 2(b). Interestingly, the metal gold tips are still observed at the end of each branches of the nanowire. The schematic diagram of formation mechanism of branched nanowires is depicted in figure 6(b). At higher growth temperature, Au droplets split into tiny nanoparticles (Liang *et al* 2001; Yan *et al* 2007). These Au droplets act as secondary nucleation centres on the nanowire surfaces, which then grow by VLS process. At higher growth temperatures, 950 and 1000°C, SnO_2 nanobelts of several micrometer length have been observed (figures 3 and 4). We propose that at a high growth temperature, the nanobelts are produced by the combination of VLS as well as VS mechanism. At 950°C, the width to thickness ratio is very large, whereas it is smaller at 1000°C. A rectangular cross-section of the SnO_2 nanobelt reveals that VLS is not the sole growth mechanism and the VS method is also dominant for the nanobelt formation. The schematic diagram of the growth of SnO_2 nanobelts is depicted in figure 6(c). It may be noted that the surface energy of the crystal plays an important role in the formation of crystal shape in the VS growth process (Beltran *et al* 2003; Wang *et al* 2003). Since the growth of SnO_2 nanobelts is initiated by the Au catalyst nanoparticles via VLS process, the size of the nanoparticles may control the thickness and morphology of resultant nanowires and nanobelts.

3.3 *X-ray diffraction study*

Figure 7 shows the grazing incidence (2·0°) X-ray diffraction patterns of the nanowires grown at different temperatures from 750–1000°C. XRD spectra show that the nanowires and nanobelts are highly crystalline with cassiterite phase (JCPDS code 77-0448), i.e. tetragonal rutile phase with lattice parameters $a = 4{\cdot}739$ Å, $b = 4{\cdot}7391$ Å and $c = 3{\cdot}1869$ Å. All the peaks for the samples grown at 850°C, 950°C and 1000°C are attributed to the SnO_2 and there is no trace of SnO and Sn phases in our nanowires and nanobelts. However, at lower growth temperature (750°C), the dominant diffraction peaks are mainly due to

cubic Au (JCPDS code 04-0784) with lattice parameters $a = b = c = 4{\cdot}0786$ Å. This is due to the poor crystallinity, low density and the shorter length of the nanowires.

3.4 *Optical properties*

The optical bandgap of SnO_2 nanowires/nanobelts were investigated using UV-visible absorption spectrometer in the wavelength range 200–800 nm. Figure 8(a) shows the typical absorption spectrum of SnO_2 nanowires grown at 850°C. The optical bandgap is found to be 3·6 eV, which is close to the bulk bandgap of SnO_2 (Camagni *et al* 2008). As the wire diameter (~80 nm) is much larger than the excitonic Bohr radius, ~2·6 nm, for SnO_2 (Yanes *et al* 2004), the bandgap enhancement due to quantum size effect is not expected. Figure 8(b) shows the room temperature photoluminescence spectra of SnO_2 nanowires/nanobelts at different growth temperatures. It may be noted that the bulk SnO_2 is not luminescent. However, nanosized SnO_2 exhibits a strong broadband luminescence attributed to surface defects and oxygen vacancies in the near-surface region (Hu *et al* 2003; Calestani *et al* 2005), although no direct evidence has been provided. The nanowires grown at 750°C and 850°C yield emission peaks at 588 and 573 nm, respectively whereas peaks at 558 and 582 nm are found in the nanobelts grown at 950 and 1000°C. In all cases, the PL emission bands are Stokes-shifted and there is no band edge emission. Figure 9 shows schematic diagram of the band structure of SnO_2 nanostructures. According to Zhou *et al* (2006) the dominated defects of the SnO_2 nanostructures are the oxygen-vacancy in the surface region. These surface states (ES) are situated ~2·7 eV below the conduction band minima (CBM) and ~0·9 eV above the valence band maxima (VBM). Besides these surface states at ES, the oxygen-vacancies also possess high electron affinity to trap electrons locally, forming oxygen vacancy-related states near CBM (Trindade *et al* 2001). The position of these states is related to the nature of the vacancy. For all growth temperatures (750–1000°C), the emission energies, 2·1–2·2 eV, are less than the energy gap between conduction band minima and surface states (~2·7 eV). So it is assumed that, in the nanowires and nanobelts, the electrons from conduction band are captured by the shallow trap levels (shown in figure 9) below the conduction band and then recombine with the hole at the surface states. Transition from surface states to valence band may be radiative or nonradiative. However, we did not investigate any radiative recombination in the IR region. FESEM micrographs clearly showed that as the growth temperature increases from 750–1000°C, the effective surface area of the wires/belts also increases. Due to the increased effective surface area of the nanowires and belts and higher oxygen vacancies, the intensity of the PL peak is found to be enhanced as a function of temperature.

Raman scattering is a useful tool for the characterization of nanosized materials and can be used as a qualitative probe to estimate the presence of lattice defects in crystalline solids. The crystalline quality can be judged from the analysis of peak shapes and the selection rules. XRD and electron diffraction pattern confirmed the formation of tetragonal rutile SnO_2 nanowires/nanobelts. The rutile SnO_2 belongs to the space group, D_{4h}^{14}, of which the normal lattice vibration at the Γ point of the Brillouin

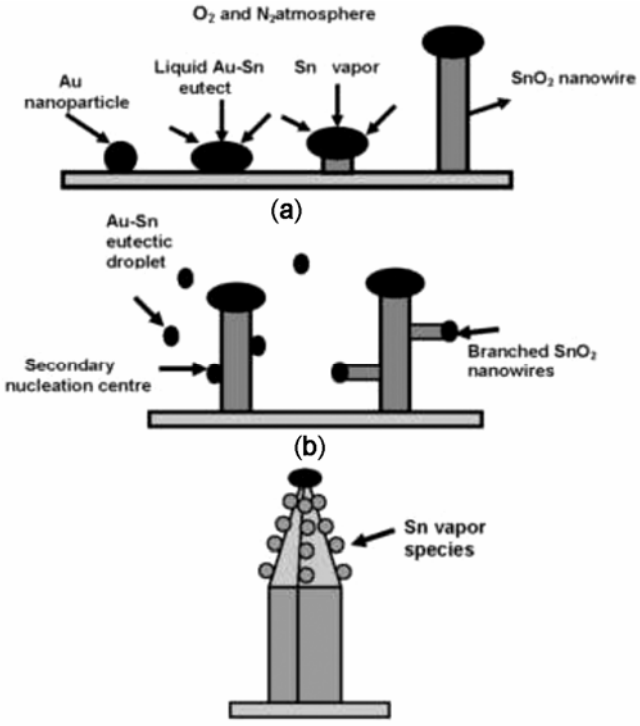

Figure 6. Schematic diagram of the growth process of SnO_2 (**a**) nanowires, (**b**) branched nanowires and (**c**) nanobelts.

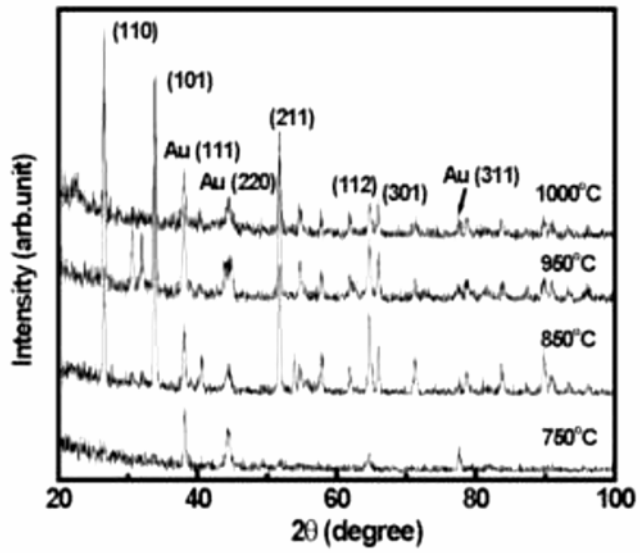

Figure 7. XRD patterns of SnO_2 nanostructures at different growth temperatures.

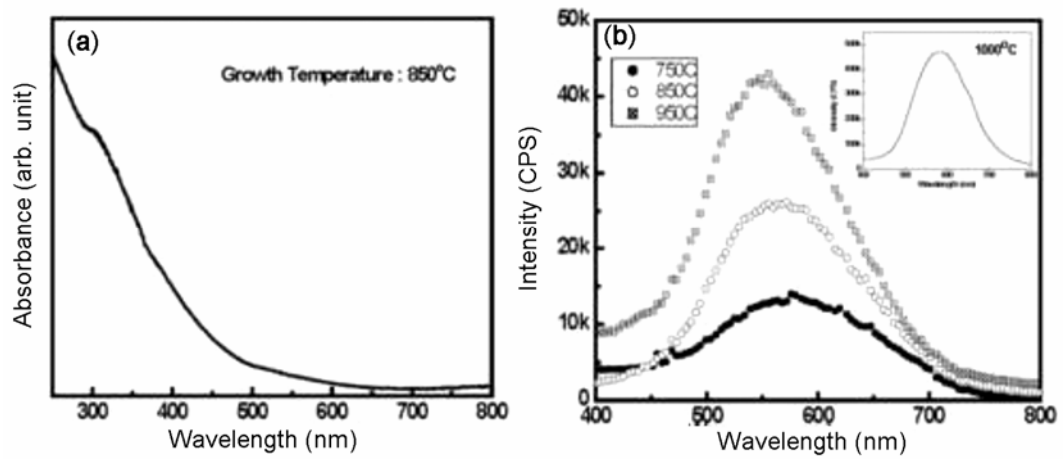

Figure 8. (**a**) Typical optical absorption spectrum of SnO_2 nanowires grown at 850°C temperature and (**b**) PL spectra of SnO_2 nanowires and nanobelts of growth temperature 750–950°C. Inset of figure **8**(**b**) shows the PL spectrum of SnO_2 nanobelts grown at 1000°C.

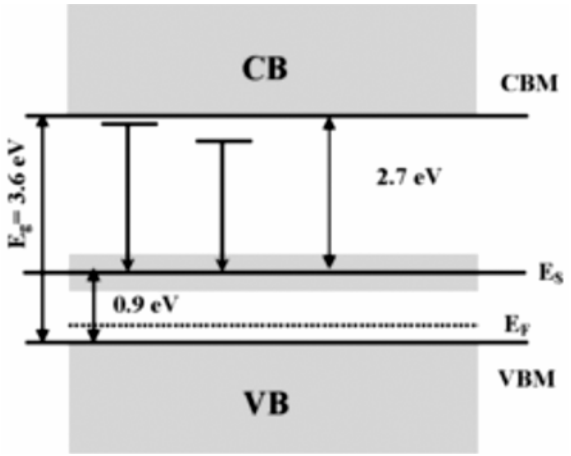

Figure 9. Schematic energy band diagram of SnO_2 nanowires and nanobelts.

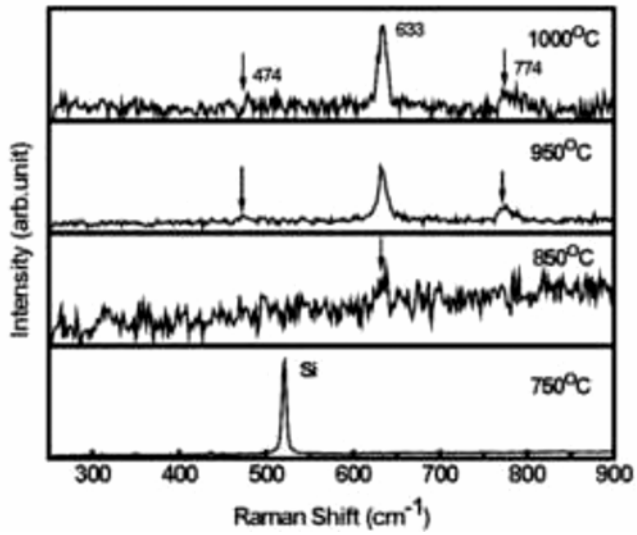

Figure 10. Raman spectra of SnO_2 nanowires and nanobelts.

zone is given on the basis of group theory (Porto *et al* 1967)

$$\Gamma = 1A_{1g} + 1A_{2g} + 1A_{2u} + 1B_{1g} + 1B_{2g} + 2B_{1u} + 1E_g + 3E_u.$$

Among them, the active Raman modes are B_{1g}, E_g, A_{1g}, and B_{2g}, and consequently four first-order Raman spectra can be observed. Figure 10 shows the room temperature Raman spectra of SnO_2 nanowires and nanobelts synthesized at different growth temperatures. At 750°C, only silicon substrate peak is visible without any characteristic Raman peak of SnO_2. At 850°C a weak peak at 633 cm^{-1} corresponding to A_{1g} Raman mode is observed. However, at higher temperatures (950–1000°C), three peaks at 474, 633 and 774 cm^{-1} corresponding to the E_g, A_{1g} and B_{2g} vibration modes, respectively are detected. These peaks confirm that the synthesized nanowires/nanobelts belong to tetragonal rutile phase (Wang *et al* 2002). The intensity of Raman peaks increases with the increase of growth temperatures. Due to the significant increase of aspect ratio and density of the wires/belts at higher growth temperatures, a larger area is available for probing of the samples and hence the remarkable increase in the peak intensities.

Figure 11 shows the Fourier transformed infrared spectra (FTIR) of SnO_2 nanowires/nanobelts with different growth temperatures. The sample prepared at 750°C shows the signatures similar to reference bulk silicon, with no visible absorption band for SnO_2. The band at 610 cm^{-1} corresponds to the phonon mode of the Si substrate (Power *et al* 2004). The absence of absorption band for 750°C growth samples is mainly due to the shortest length of nanowire. However, at higher growth temperatures (850–1000°C) several bands around 1086, 688, 610, 563 and 467 cm^{-1} are observed. The peaks at 688 and 563 cm^{-1} correspond to the characteristic signatures of

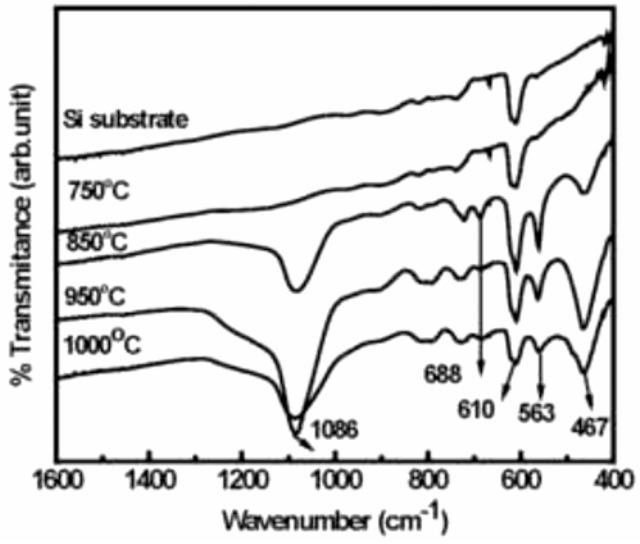

Figure 11. FTIR spectra of SnO_2 nanowires and nanobelts at different growth temperatures.

SnO_2 (Amalric-Popescu and Bozon-Velduraz 2001). The most important IR feature is the peak at 563 cm^{-1}, due to the surface mode of SnO_2 nanowires and nanobelts (Peng *et al* 2003). However, at higher growth temperatures, 850–1000°C, two distinct and well-defined bands at 467 and 1086 cm^{-1} are observed due to rocking and asymmetric stretching modes of Si–O–Si band, respectively (Ye *et al* 2002). At higher temperature the silicon substrate is oxidized due to the presence of oxygen in nitrogen atmosphere.

4. Conclusions

We have successfully grown SnO_2 nanowires and nanobelts at different growth temperatures (750–1000°C). SEM and TEM micrographs revealed the formation of different types of nanostructures. It was also investigated that the structural morphology changes from wire to belt with the increase of growth temperature. In our growth process, the nanowire growth is mainly due to the vapour–liquid–solid growth process, but both the VLS as well as VS process play an important role in the formation of nanobelts. As-prepared SnO_2 nanostructures are highly crystalline with tetragonal rutile phase and there is no elemental trace of Sn and SnO, which was verified by XRD and selected area electron diffraction pattern. The optical bandgap of the nanowires yields the bulk bandgap value ~3·6 eV of SnO_2. PL emission shows a broad emission (558–588 nm), which is attributed to the oxygen deficiency present in the nanostructures. The intensity of the Raman peak increases with growth temperature due to increasing aspect ratio of the nanowires and nanobelts. FTIR spectra exhibit characteristic signatures of SnO_2 with peaks at 688 and 563 cm^{-1} and that at 563 cm^{-1} is attributed to the surface mode of SnO_2.

Acknowledgements

This work was supported in part by a nanoinitiative project grant of the Department of Science and Technology (grant no. SR/S5/NM-04/2005). One of the authors (SPM) acknowledges the Council of Scientific and Industrial Research, Government of India, for an SRF fellowship.

References

Amalric-Popescu D and Bozon-Verduraz F 2001 *Catal. Today* **70** 139
Ansari G, Boroojerdian P, Sainkar S R, Karekar R N, Aiyer R C and Kulkarni S K 1997 *Thin Solid Films* **295** 271
Beltran A, Andres J, Longo E and Leite E R 2003 *Appl. Phys. Lett.* **83** 635
Calestani D, Lazzarini L, Salviati G and Zha M 2005 *Cryst. Res. & Technol.* **40** 937
Camagni P *et al* 1996 *Sens. Actuators* **B31** 99
Comini E, Faglia G, Sberveglieri G, Pan Z and Wang Z L 2002 *Appl. Phys. Lett.* **81** 1869
Dai Z R, Pan Z W and Wang Z L 2001 *Solid State Commun.* **118** 351
Dattoli E N, Wan Q, Guo W, Chen Y, Pan X and Lu W 2007 *Nano Lett.* **7** 2469
Duan J, Yang S, Liu H, Gong J, Huang H, Zhao X, Zhang R and Du Y 2005 *J. Am. Chem. Soc.* **127** 6180
Duan X F, Huang Y, Cui Y, Wang J and Leiber C M 2001 *Nature* (*London*) **409** 66
Ferrere S, Zaban A and Gsegg B A 1997 *J. Phys. Chem.* **B101** 4490
He J H, Wu T H, Hsin C L, Li K M, Chen L J, Chueh Yu L, Chou L J and Wang Z L 2006 *Small* **2** 116
Her Y C, Wu J Y, Lin Y R and Tsai S Y 2006 *Appl. Phys. Lett.* **89** 043115
He Y S, Cambell J C, Murphy R C, Arendt M F and Swinnea J S 1993 *J. Mater. Res.* **8** 3131
Hu J Q, Bando Y, Liu Q L and Golberg D 2003 *Adv. Funct. Mater.* **13** 493
Kolmakov A, Klenov D O, Lilach Y, Stemmer S and Moskovits M 2005 *Nano Lett.* **5** 667
Liang C H, Meng G W, Wang G Z, Wang Y W and Zhang L D 2001 *Appl. Phys. Lett.* **78** 3202
Ma Y J, Zhou F, Lu L and Zhang Z 2004 *Solid State Commun.* **130** 313
Pan Z W, Dai Z R and Wang Z L 2001 *Science* **291** 1947
Peng X S, Zhang L D, Meng G W, Tian Y, Lin T Y, Geng B Y and Sun S H 2003 *J. Appl. Phys.* **93** 1760
Porto S P S, Fleury P A and Damen T C 1967 *Phys. Rev.* **154** 522
Power G, Vij J K and Shaw M 2004 *J. Phys. D: Appl. Phys.* **37** 1362
Sears G W 1955 *Acta Metall.* **3** 361
Trindade T, Brien P O and Pichett N L 2001 *Chem. Mater.* **13** 3834
Varghese O K and Malhotra L K 1998 *Sens. Actuators* **B53** 19
Wagner R S and Ellis W C 1964 *Appl. Phys. Lett.* **4** 89
Wang J X *et al* 2004 *Solid State Commun.* **130** 89

Wang W Z, Xu C K, Wang G H, Liu Y K and Zheng C L 2002 *J. Appl. Phys.* **92** 2740
Wang Z L, Kong X Y and Zuo J M 2003 *Phys. Rev. Lett.* **91** 185502
Wu Y and Yang P J 2001 *J. Am. Chem. Soc.* **123** 3165
Xia Y, Yang P, Sun Y, Wu Y, Mayers B, Gates B, Yin Y, Kim F and Yan H 2003 *Adv. Mater.* (*Weinheim, Germany*) **15** 353
Yanes A C *et al* 2004 *Appl. Phys. Lett.* **85** 2343
Yang P and Lieber C M 1997 *J. Mater. Res.* **12** 2981
Yan Y, Zhang Ye, Zeng H, Zhang J, Cao X and Zhang L 2007 *Nanotechnology* **18** 175601
Ye C N, Wu X M, Tang N Y, Zhuge L J, Yao W G, Chen J, Dong Y M and Yu Y H 2002 *Sci. & Technol. Adv. Mater.* **3** 257
Zheng M, Li G, Zhang X, Huang S, Lei Y and Zhang L 2001 *Chem. Mater.* **13** 3859
Zhou X T, Heigl F, Murphy M W, Sham T K, Regier T, Coulthard I and Blyth R I R 2006 *Appl. Phys. Lett.* **89** 213109